

Discovery of Charge Density Wave Order in the Topological Insulator Bi_2Se_3

Yanan Li¹, Christian Parsons¹, Sanath Kumar Ramakrishna², Anand Prashant Dwivedi¹, Marvin A. Schofield¹, Arneil P. Reyes², and Prasenjit Guptasarma¹

¹Department of Physics, University of Wisconsin-Milwaukee, Milwaukee, Wisconsin 53211, USA ²National High Magnetic Field Laboratory/Florida State University, Tallahassee, Florida 32310, USA

Abstract

Hexagonally deformed Fermi surfaces and strong nesting, found in topological insulators (TIs) such as Bi_2Se_3 and Bi_2Te_3 over the past decade, have led to several predictions of the existence of Density Wave order in these systems. Recent evidence for strong Fermi nesting in superconducting $\text{Cu-Bi}_2\text{Se}_3$ and $\text{Nb-Bi}_2\text{Se}_3$ has further led to the speculation about the importance of charge order in the context of unconventional superconductivity. Here, we report what we believe is the first direct observation of Charge Density Wave (CDW) order in Bi_2Se_3 . Our results include the observation of a 140K metal-insulator-metal transition in resistivity as a function of temperature. This is corroborated by nuclear magnetic resonance (NMR) studies of the spin-lattice relaxation ($1/T_1$) rate of the ^{209}Bi nucleus, which also displays a transition at 140K associated with an opening of an energy gap of $\sim 8\text{meV}$. Additionally, we use electron diffraction to reveal a periodic lattice distortion (PLD) in Bi_2Se_3 , together with diffuse charge order between \vec{k} and $\vec{k} \pm \Delta\vec{k}$. This diffuse scattering points toward the presence of an incommensurate charge density wave (I-CDW) above room temperature, which locks into a CDW upon cooling below $\sim 140\text{K}$. We also observe an additional transition in $1/T_1$ near 200K, which appears to display anisotropy with the direction of applied magnetic field. In this report, we focus on

the CDW transition at 140K and include some speculation of the other transition observed at 200K by NMR, also revealed here for the first time.

Introduction

The 2D layered chalcogenide Bi_2Se_3 and its intercalated versions continue to elicit significant interest due to the presence of non-trivial topological surface states protected by time reversal symmetry, along with fascinating properties of nematic order and superconductivity.¹⁻⁶ Ideally, Bi_2Se_3 is a 3D topological insulator with a single Dirac cone within a substantial bulk energy gap (0.3 eV).⁷ However, several experiments have observed a lowering of the bulk conduction band due to natural electron doping from vacancies or antisite defects crossing the Fermi energy and allowing for bulk electron conduction.⁸⁻¹¹ Under high pressure, or upon intercalating with metals such as Cu and Nb, Bi_2Se_3 displays unconventional superconductivity.¹²⁻¹⁴ Most unconventional superconductivity arises out of strong electron-electron correlations.¹⁵⁻¹⁸ However, Bi_2Se_3 displays weak *sp* electron correlation.^{19,20} This conundrum has led to a search for other possible mechanisms for unconventional electron pairing in Cu-, Sr- and Nb- intercalated Bi_2Se_3 . An idea that has gained ground in recent years is based on Fermi nesting. First principle calculations on $\text{Cu}_x\text{Bi}_2\text{Se}_3$, in combination with elastic neutron diffraction measurements on $\text{Sr}_{0.1}\text{Bi}_2\text{Se}_3$, indicate that singular electron-phonon interactions with strong Fermi nesting at long wavelength can lead to pseudo-triplet pairing with A_{2u} symmetry.^{1,2} In addition to this, there is now strong evidence that with contributions from the bulk, the cross section of the Dirac cone in Bi_2Se_3 evolves from circular geometry at the Dirac point into a hexagon-like geometry around 350 meV above the Dirac point, and

eventually to a hexagram-like geometry near 435 meV above the Dirac point.²¹ The near-flat pieces of such a hexagon in the range $0.55E^* < E < 0.9E^*$ can result in nesting vectors at $Q_i = 2k_{Fe_i}$, $i=1 \dots 3$, where Q_i is the wave vector and k_{Fe_i} is the Fermi momentum.²² Central to a strong Fermi nesting factor is the layered structure of Bi_2Se_3 . Angle-resolved Photoemission Spectroscopy (ARPES) studies on Bi_2Se_3 have confirmed that natural electron-doped Bi_2Se_3 has a hexagonally deformed Fermi Surface. Kuroda et al²¹ have suggested that two flat segments of a hexagonal Fermi surface facing each other across $2\vec{k}_F$ along $\vec{\Gamma} - \vec{k}$ could lead to strong nesting. One of the possible outcomes of such Fermi nesting is the appearance of Density Waves. Realistically, this is a deviation from an ideal TI, which has a single Dirac cone with a circular Fermi surface,²³ and in which the formation of a charge density wave, or a spin density wave, is forbidden. A few studies have hinted at the existence of CDWs in Cu- Bi_2Se_3 , but so far there has been no evidence of a gap opening with temperature variation, indicating a CDW transition.²⁴⁻²⁶ Additionally, there have been no such reports in Bi_2Se_3 . Here, we report for the first time that Bi_2Se_3 undergoes a transition to a CDW state at 140K.

The ground state of a charge density wave (CDW), which is observed mostly in low dimensional materials, is characterized by spontaneously broken translational symmetry. In the simplest case, the 1D Peierls transition can be a first order or a second order transition characterized by the temperature evolution of the order parameter. In real life, and in more complex systems, the phase transition to a CDW ground state is mostly observed together with commensurate/incommensurate Periodic Lattice Distortions (PLD) concomitant with the opening of an energy gap at the Fermi level, resulting in a metal-to-insulator like transition in resistivity as a function of temperature. Single crystals

with *imperfect chains* (quasi-1D), or *imperfect nestings* (quasi-2D), can lead to such an energy gap being partially opened. In such situations, a CDW tends to co-occur with a PLD²⁷⁻²⁸ such that the PLD and the CDW are commensurate with the periodicity of the underlying atomic lattice distorted by the PLD. The electronic charge density, which is a scalar quantity and mostly used as an order parameter of a CDW, is coupled with the PLD. In such a situation, the ordered CDW possesses a period that is an integral or a fractional multiple of the period of either the atomic lattice or the PLD. In cases where the CDW periodicity is not represented in the reciprocal lattice by specific vectors \vec{k} , but rather by an entire range of vectors $\vec{k} \pm \Delta\vec{k}$, one observes diffraction patterns with ‘diffuse’ intensity centered around \vec{k} , and often between Bragg reflections, while maintaining the overall symmetry of the underlying lattice. This is a signature of an incommensurate CDW, or I-CDW,^{27,28} which often precedes a commensurate CDW transition at lower temperature. Our electron diffraction results point to the possibility that an I-CDW might already exist in Bi₂Se₃ above room temperature.

We report here a combination of resistivity, Selected Area Electron Diffraction (SAED) and Nuclear Magnetic Resonance (NMR) studies to reveal that Bi₂Se₃ undergoes a transition to a CDW state at 140K. We observe a 140K metal-insulator-metal transition in resistivity as a function of temperature. Our measurements of the NMR spin-lattice relaxation ($1/T_1$) rate of the ²⁰⁹Bi nucleus also shows an anomaly at 140K, with an energy gap approximately 8meV. Additionally, electron diffraction reveals a periodic lattice distortion (PLD) in Bi₂Se₃ as well as diffuse charge order between \vec{k} and $\vec{k} \pm \Delta\vec{k}$, as described in the previous paragraph. We argue that this diffuse scattering arises from an incommensurate charge density wave (I-CDW) at higher temperature, foreshadowing a

transition to CDW order, into which the I-CDW locks upon cooling below $\sim 140\text{K}$. We also identify another transition in NMR $1/T_1$ near 200K which is anisotropic with applied magnetic field. Comparison of relaxation rates $\Delta 1/T_1$ from $H\parallel c$ to $H\perp c$, with $\Delta 1/T_1 = 1/T_1(\parallel) - 1/T_1(\perp)$, again signifies this transition indicating that a stronger lattice vibration (phonons) is present in the $H\parallel c$ -axis measurements. Therefore, it is likely that the transition at 200K is a phonon mediated structural phase transition.

Results

Electron and X-ray Diffraction

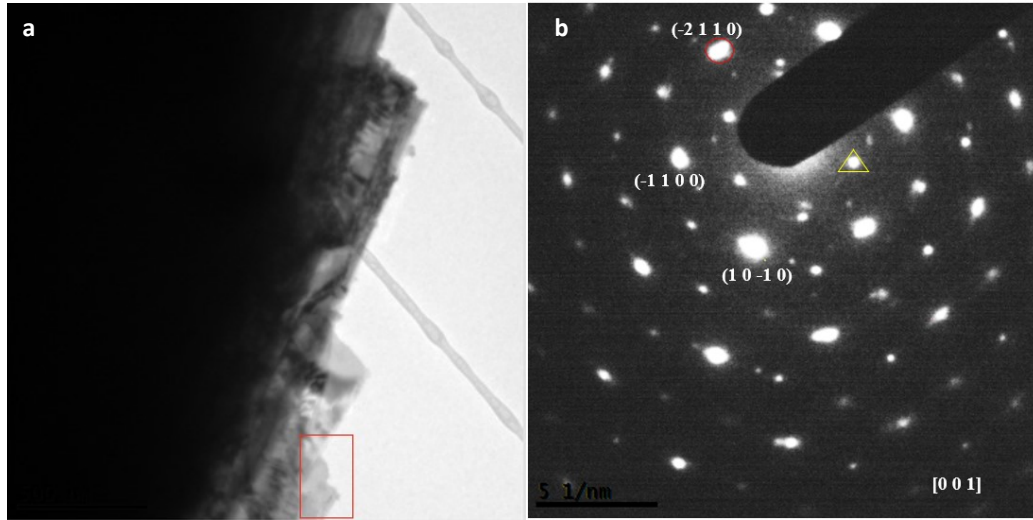


Fig. 1 Transmission Electron Microscopy (TEM) and Selected Area Electron Diffraction (SAED) studies on Bi_2Se_3 single crystal at room temperature. **a** Bright field image of a piece from single crystal of Bi_2Se_3 . The red box indicates the region on which SAED was performed. **b** Electron diffraction along $[001]$ zone axis. Weak reflections of the type identified by a yellow triangle represent normally forbidden reflections from $3a/2$ reflections in the $[001]$ zone axis. Relatively strong reflections, circled in red, are identified reflections from the $[001]$ zone axis.

Fig. 1 and Fig. 2 show Selected Area Electron Diffraction (SAED) performed on

Bi_2Se_3 at room temperature. Fig. 1a shows the area from which the diffraction pattern in Figure 1b was obtained along the [001] zone axis. Note the alternate bright and dim spots in Fig. 1b, with high-intensity spots identified and circled in red. These features were also observed in SAED by Koski, et al and Wang, et al.^{24,29} Both groups studied the result of intercalation of different zero-valent metals into the van der Waals gaps in Bi_2Se_3 . They suggest that the most likely reason for the appearance of these weak intensity spots, otherwise forbidden in the cubic-like ABC [001] zone axis in the host Bi_2Se_3 lattice, is the result of a stacking fault. In other words, the presence of zero-valent intercalants in the van der Waals gap can alter inter-planar energetics in such a way as to stabilize hexagonal stacking relative to rhombohedral stacking, resulting in a high density of stacking faults.

The process of self-intercalation has previously been discussed by other authors.^{30,31} Rietveld fitting of X-ray diffraction (XRD) on our Bi_2Se_3 samples reveals that the $a(=b)$ axis value is 4.14 Å, which agrees with other reports. However, we find that our c -axis value is 28.66 Å. This is 0.02 Å higher than the 28.64 Å reported in most previous experiments on Bi_2Se_3 . Previous authors have discussed that a longer c -axis, with values as high as 28.65 Å, can arise from the unintended intercalation of Bi into the van der Waals gap as a neutral metal Bi_2 layer.³⁰ Analyzing the XRD peak broadening based on Williamson-Hall analysis method,^{32,33} presented in the supplemental materials, demonstrates lattice strain in our Bi_2Se_3 sample. The measured isotropic strain is consistent with point defects, and further supports our assertion of Bi intercalation or Se vacancies. Based on the higher c -axis value in our samples, and our evidence for stacking faults in SAED, we suggest that the van der Waals gaps in our Bi_2Se_3 crystals

have zero-valent Bi or Se metal resulting from “self-intercalation.” The consequences of this are discussed later in this paper.

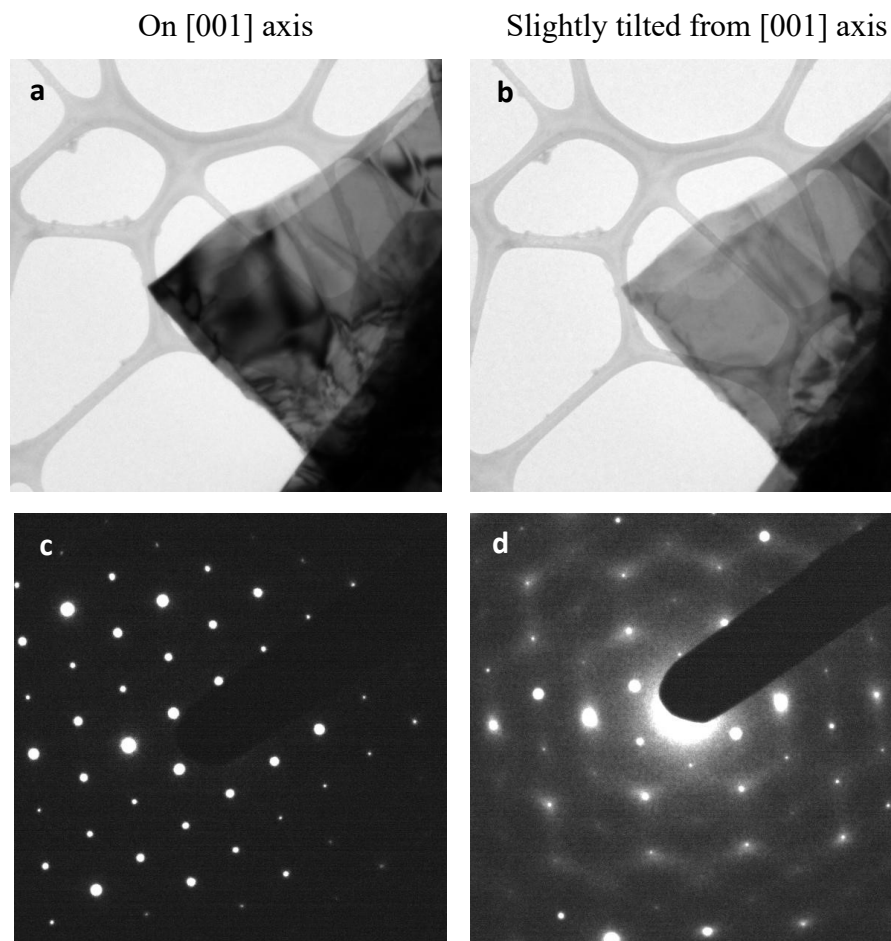


Fig. 2 **a, b** Bright field TEM on a flake obtained from single crystal Bi₂Se₃. **c, d** Selected Area Electron Diffraction from the corresponding areas shown in (a) and (b). The images in (a) and (c) show results when the beam is on [001] axis. Images in (b) and (d) show off-axis electron diffraction, for which the sample was tilted slightly (less than 5 degrees) away from zone axis.

Fig. 2 displays bright field TEM and SAED on flakes obtained from single crystal Bi₂Se₃. Fig. 2a, c are bright field images on the [001] zone axis. Fig. 2b, d are taken from the same region of the flake, with the sample tilted slightly (less than 5 degrees) away from the zone axis. The images in Fig. 2c, d correspond to the areas shown in Fig. 2a, b,

respectively. As can be seen in Fig. 2d, the diffraction pattern with the crystal tilted slightly off the [001] zone axis yields diffuse streaks between the diffraction spots. As discussed in previous reports on other similar layered compounds,^{27-28, 34-37} our interpretation is that this diffuse intensity is due to Periodic Lattice Distortion (PLD) associated with an incommensurate charge density wave (I-CDW), which often occurs as a precursor to a charge density wave (CDW).²⁷

Resistivity measurements

Four-probe DC resistivity measurements, shown in Fig. 3 and Fig. 4, were performed in the 2K-300K temperature range with linearly aligned electrodes on the *ab* surface of Bi₂Se₃ single crystals, and with the electric field $E \parallel ab$. To ensure reproducibility, we performed measurements on several different pieces of as-grown single crystal. Fig. 3a, b, are results on different pieces from the same batch of as-grown single crystal.

Resistivity measurements at zero field all show approximately metallic behavior from room temperature down to around 140 K. Note a sharp upturn in resistivity with decreasing temperature, centered around 140K, followed by a return to metal-like behavior below 140K. In Fig. 3a, with cooling, we see a rise in resistivity from $\sim 1.38 \times 10^{-5} \Omega\text{m}$ to $1.47 \times 10^{-5} \Omega\text{m}$; in Fig. 3b, we observe a rise of $\sim 1.31 \times 10^{-5} \Omega\text{m}$ to $1.36 \times 10^{-5} \Omega\text{m}$, followed in both cases by a return to metal-like behavior at lower temperature. The insets to Fig. 3a,b show dp/dT as a function of temperature, clarifying the inflection point and onset near 140K. We identify this metal-insulator-metal behavior as resulting from a gap or instability at the Fermi level, correlated with a transition to a CDW ground state.^{38,39}

Heating and cooling cycles performed on the second piece of Bi_2Se_3 shown in Fig. 3b display very weak thermal hysteresis behavior above the onset transition temperature 140K, pointing to the possibility that the 140K transition is an unconventional second order CDW transition.^{40,41} On the other hand, the hint of a thermal hysteresis (between heating and cooling) in resistivity above 200K, shown as a solid red line and a dashed blue line in Fig. 3b, points to the presence of a possible first order transition at higher temperature. We believe that this could arise from a transition from normal phase to an incommensurate charge density wave phase at some temperature above room temperature.⁴² This agrees with our room-temperature electron diffraction data described below, in which we observe the presence of an I-CDW phase. We therefore assign the transition at 140K to a second order transition from I-CDW to CDW. The lack of (or, weak) thermal hysteresis at 140K indicates a possible phonon-mediated unconventional mechanism described further in the discussion section.^{1,2,43,44}

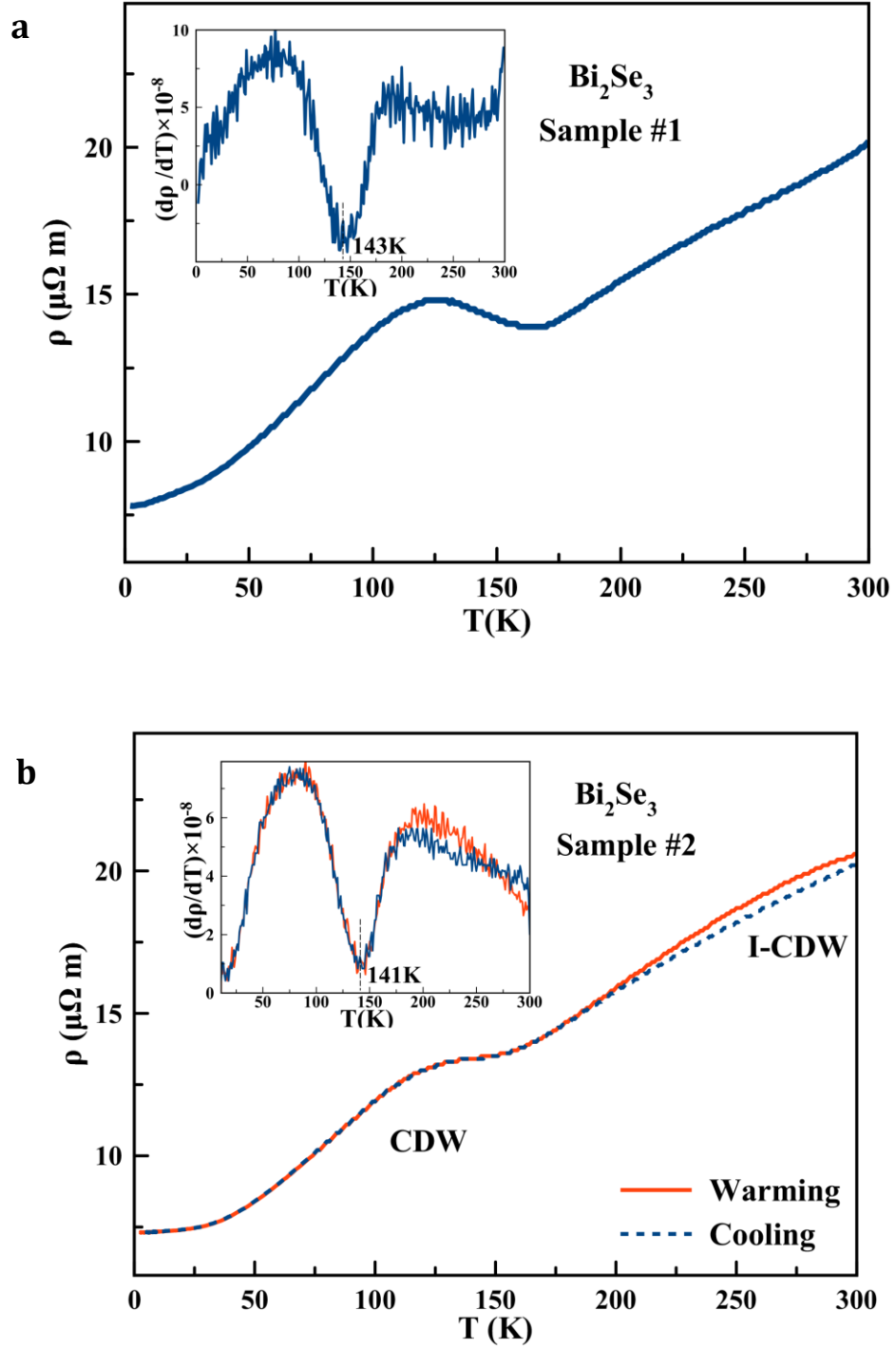


Fig. 3 Resistivity of Bi_2Se_3 as a function of temperature for two different pieces, sample#1 and sample#2, measured in zero magnetic field with the electric field along the ab plane. **a** Measurement on sample #1 while cooling the sample from 300 K to 2 K; **b** Measurement on sample#2 for both cooling and heating.

Insets for **a** and **b** are the plots of dp/dT as a function of temperature to clarify the temperature values of the inflection points and the CDW transition temperature T_{CDW} .

Fig. 4 examines the magnetic field dependence of the CDW transition temperature (T_{CDW}) for sample#2, same sample as the one shown in Fig. 1b, with magnetic field $H \parallel c$ -axis varying between 0.00T and 4.50T. The inset in Fig. 4 displays dp/dT as a function of T , indicating that the transition temperature does not change with applied magnetic field H below 5T. This result is similar to the one obtained for an unconventional CDW in $La_3Co_4Sn_{13}$, and is also consistent with our NMR results discussed in subsequent sections.⁴⁰

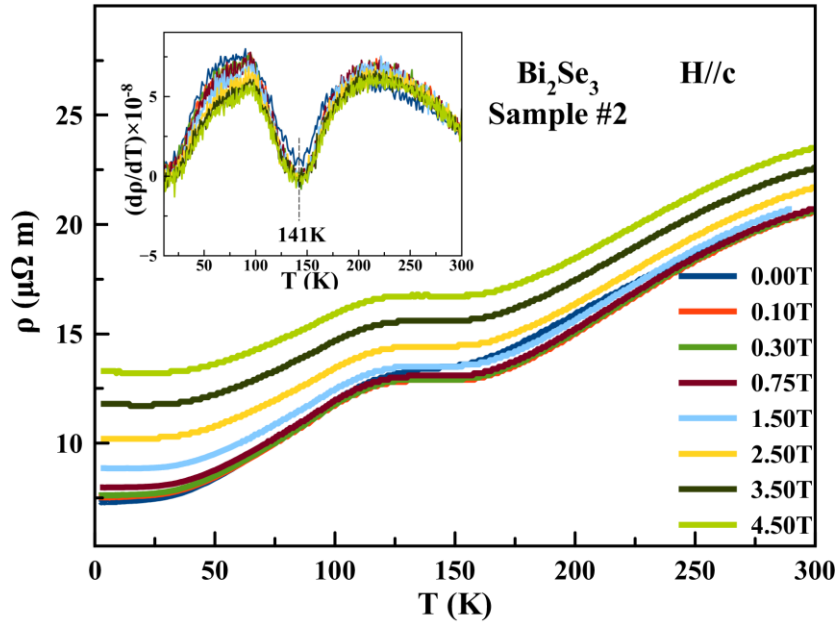


Fig. 4 Thermal dependence of resistivity of Bi_2Se_3 for different values of applied magnetic field $H \parallel c$ -axis varying between 0.00 – 4.50 Tesla.

Nuclear Magnetic Resonance

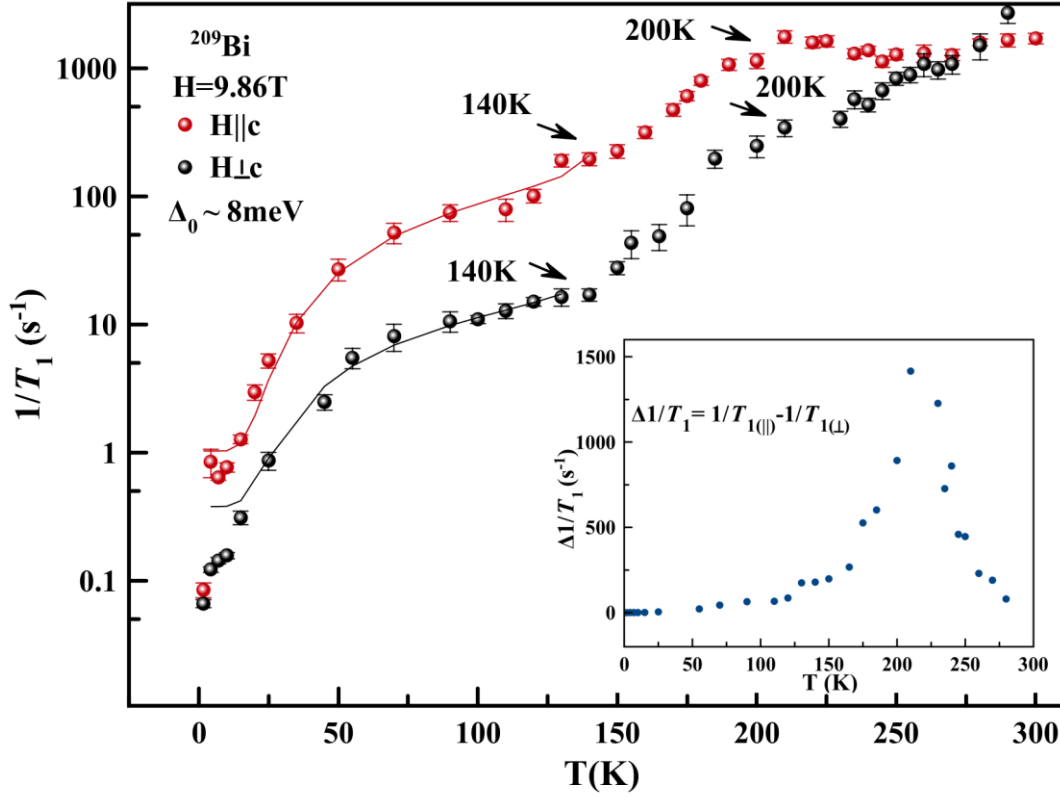


Fig. 5 Spin-lattice relaxation rate ($1/T_1$) shown with temperature T varying between 1.6K and 300K with applied magnetic field directions: $H \parallel c$ -axis (red balls) and $H \perp c$ -axis (black balls). Arrows indicate possible transitions at 140K, and 200K in each direction, where the 140K is the commensurate CDW transition temperature. Solid lines are fits to a temperature-dependent CDW energy gap Δ_0 , with gap value $\sim 8\text{meV}$. Inset: Differences of $1/T_1$ from the two magnetic field orientations as a function of temperature where $\Delta 1/T_1 = 1/T_{1(\parallel)} - 1/T_{1(\perp)}$. We see the largest difference occurring at 200K.

In order to provide a microscopic information about the nature of these transitions, we performed NMR relaxation measurements. The nuclear spin-lattice relaxation rate $1/T_1$ measures the recovery of the longitudinal nuclear magnetization following an external

perturbation such as an RF field. The magnetization recovery $M(t)$ is fitted with a stretched single exponential (see methods). However, we find that the fits with and without the stretch parameter gives similar T_1 results, giving stretched component β values close to 1. The results of this fit are shown in Fig.5. Figure 5 displays the temperature dependence of $1/T_1$ of the central $|\pm 1/2\rangle \leftrightarrow |\mp 1/2\rangle$ transition of the ^{209}Bi nuclei ($I = 9/2$), with temperature varying from 1.6K to 300K, and with the external magnetic field $H = 9.86\text{T}$ applied in two orientations, $H \parallel c\text{-axis}$ and $H \perp c\text{-axis}$. It is clear that the spin-lattice relaxation rate $1/T_1$ for both field orientations follows similar behavior as a function of temperature. Although the relaxation rates for $H \parallel c$ are about an order of magnitude longer when compared to $H \perp c$, they approach nearly the same value at room temperature.

In Fig. 5, we see two obvious slope changes: at 140K and at 200K, indicated by arrows. The 140K anomaly coincides with the metal-insulator-metal transition observed in our resistivity measurements which we interpreted earlier as a transition to a commensurate CDW state. The sudden downturn of $1/T_1$ below 140K suggests an opening of an energy gap due to the formation of CDW state below this temperature. The T_1 data is then fitted to a BCS-like gap equation, as shown in Fig. 5. The obtained CDW gap value, $\sim 8\text{meV}$, is isotropic as it is independent of the direction of the magnetic field. The anomaly seen at 200K exhibits a weak anisotropy with applied magnetic field. In the inset of Fig. 5 we show the anisotropy of the relaxation rate, $\Delta 1/T_1$ as a function of temperature. The anisotropy starts small at room temperature and grows as the temperature is lowered, peaking at 200K before decreasing again towards zero at base temperature. The 140K gap and 200K anomaly are described more in detail in the following discussion section.

Discussion

The exact nature of Fermi surface distortion, nesting, and density wave instability in a system such as Bi_2Se_3 is critically dependent upon the details of its fermiology.

Correlated electron systems typically exhibit intertwined electronic ordered states resulting from several degrees of freedom such as lattice, charge, dimensionality, nematicity, and spin – all of which, in turn, tend to be strongly materials-dependent.

Many properties of chalcogenides such as Bi_2Se_3 arise from the nature of fluctuations, or overlaps in order parameter, among such intertwined orders. The severity of the overlap tends to be materials-dependent as well. Below, we discuss how materials aspects of Bi_2Se_3 , specifically, can lead to multiple ground states such as that of a charge density wave (CDW). Further, the proximity of superconductivity and density wave orders in many materials begs a discussion of the observed CDW in the context of superconductivity in Bi_2Se_3 , which we think is critical to the understanding of charge order, superconductivity, as well as nematicity in these families.⁴⁵ In this section, we begin with a discussion of the two different transitions found in our measurements. We end by describing important materials considerations which, we believe, drive the multiple (possibly intertwined) order parameters in this layered chalcogenide.

Transition near 140 K:

Nuclear relaxation measurements, in Fig. 5, together with resistivity measurements in Fig. 3 and Fig. 4 clearly reveal a transition near 140K. We interpret this as a transition to

a CDW state below 140K. We support this conclusion from electron diffraction measurements at room temperature (Fig. 1 and Fig. 2), which reveal the presence of a periodic lattice distortion (PLD) combined with diffuse scattering in off-axis diffraction, suggesting the presence of an incommensurate charge density wave (I-CDW) state already at room temperature. Interestingly, T_1 anomalies have been associated with CDW transition in layered systems.⁴⁶⁻⁴⁹

Below 140K, the CDW gap may be determined from the relaxation rate, as follows:^{50,51}

$$1/T_1 = a \exp[-\Delta(T)/T] + c \quad (1)$$

where we shall use the form of T-dependent BCS gap equation:

$$\Delta(T) = \Delta_0 \tanh(1.74 \sqrt{\frac{T_c}{T} - 1}) \quad (2)$$

Here, $T_C = T_{CDW}$ is the CDW transition temperature, a and c are fitting constants. The fit (Fig. 5) yields a zero-temperature energy gap of $\Delta_0 = 8 \pm 2 \text{ meV}$ in both directions of applied field. We estimate our coupling constant $\lambda = \Delta_0/k_B T_{CDW} = 0.7$ (where $T_{CDW} = 140 \text{ K}$ and k_B is the Boltzmann constant) which is close to the weak coupling limit. In the weak coupling limit, coupling constant $\lambda \sim 1.7$.

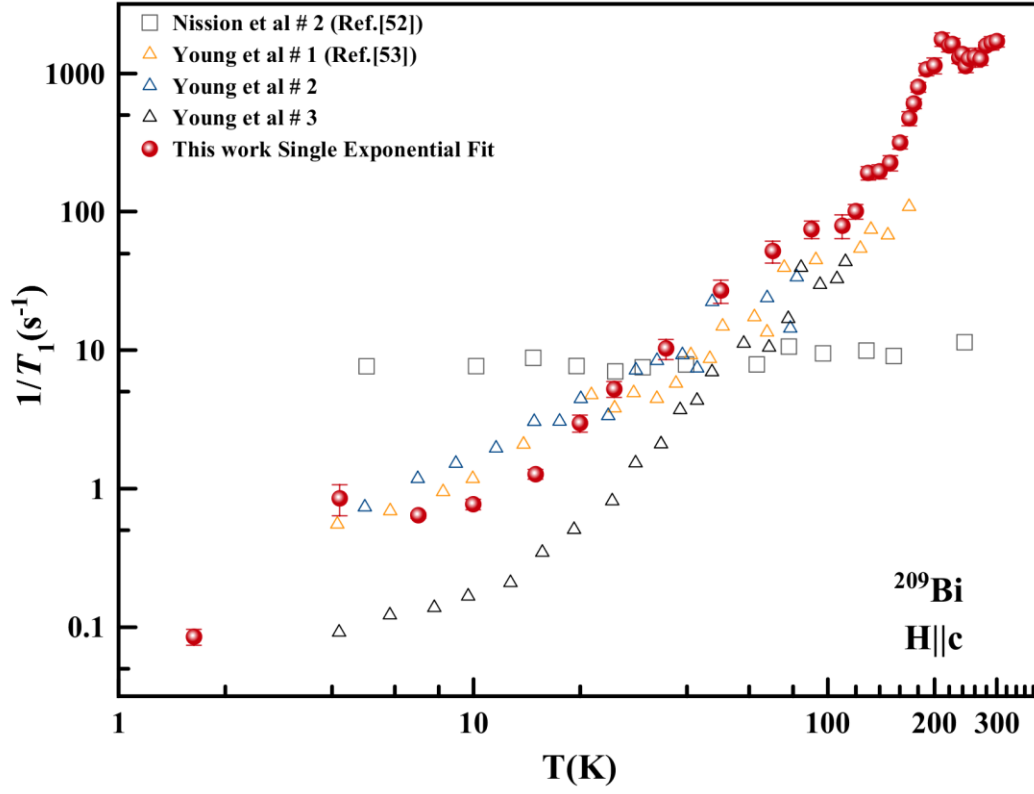


Fig. 6 Comparison of Spin-lattice relaxation rates of ^{209}Bi versus temperature from earlier published papers to our results in the magnetic field $\text{H}||\text{c}$ direction. The open data points are reproduced from Ref. [52] (square shapes from Nisson's sample #2, most of Nisson's results are in the same range) and Ref. [53] (triangle shapes, sample #1, #2 and #3). Solid data points are our results same as displayed in Fig. 5 $\text{H}||\text{c}$ direction data, with single exponential fit.

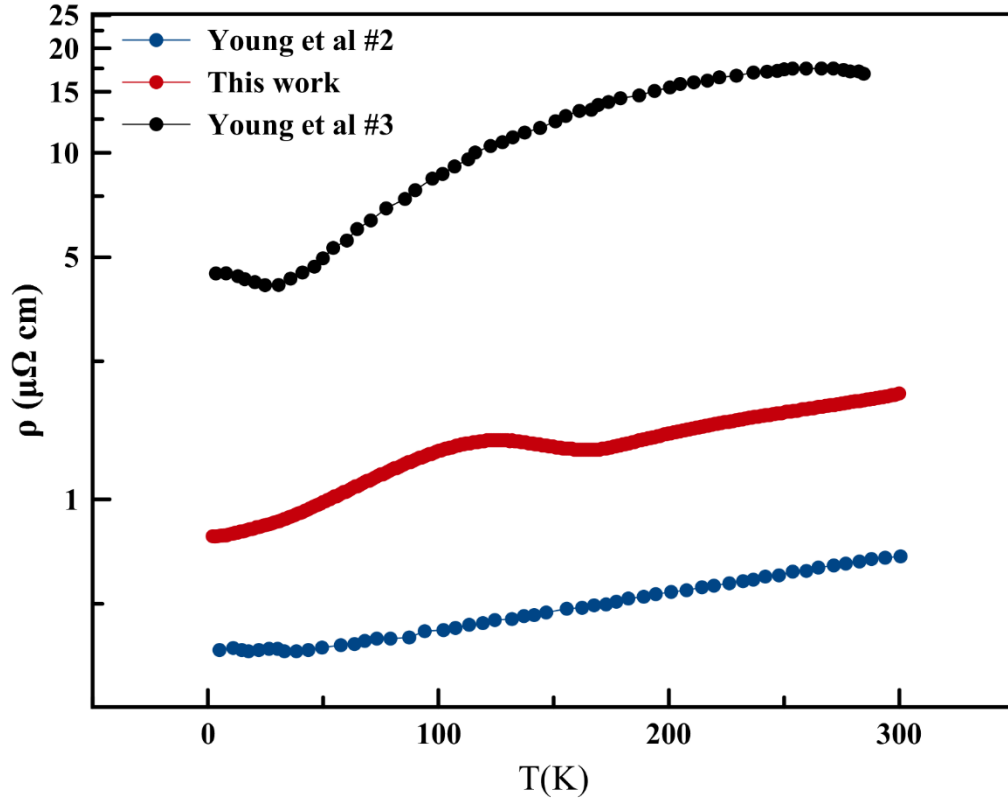


Fig. 7 Comparison of resistivity vs temperature results from our transport measurement (red) and from Ref. [53] Young et al (sample #2 blue and sample #3 black).

Previous relaxation measurements show a large variation in magnitudes and temperature dependences across samples prepared using various methods.^{52,53} These variations were attributed in part to the level of defects associated with Se-vacancies which could shift the Fermi level by partially occupying the conduction band. Unlike previous studies, our data shows a very strong temperature dependence from 1.6 to 300K, spanning almost 4 orders of magnitude for H₁c. (see Fig. 6- all T_1 data) The low-temperature behavior (below 50K) is comparable to that of sample #2 of Ref. [53] which the authors identify as

the sample with higher carrier concentration. Further, comparison of the resistivity data (Fig. 7-composite plot of ρ from ref. Young and this work) shows that our sample has slightly less carriers than Young's sample #2 but far from insulating, suggesting that the Fermi level sits lower in the conduction band. This is consistent with our NMR linewidth, and Knight shift whose values lie in between Young's samples #2 and #3. For example, our $K_{\text{iso}} \sim 0.4\%$ while Young's #2 is $\sim 0.65\%$ and Young's #3 is $\sim 0.34\%$ at 4.2K. An argument can be made that it is possible that in some direction of the reciprocal space that half band-filling, essential for Peierls transition, has been serendipitously achieved in our sample by appropriate doping through Se-vacancies leading to the formation of CDW in our sample but not in others.

Transition near 200K:

The transition near 200K merits further discussion in light of the fact that Debye temperature is $\Theta_D \approx 182\text{K}$ for Bi_2Se_3 .⁵³ Given that the behavior of $1/T_1$ is dependent upon the details of the high temperature phonon spectrum, one would expect it to behave differently above and below the Debye temperature. Thus, it is plausible that the transition observed around 200K in Fig. 5 is due to changes in the phonon spectrum across Θ_D . However, note the anisotropy in this transition with the direction of applied magnetic field, $H \parallel c$ and $H \perp c$, as is clear from Figure 5.

In Fig.3b, we observe a thermal hysteresis in resistivity above 182K. Whereas a transition across Θ_D would yield a change in slope of resistivity, we are hard-pressed to explain the thermal hysteresis in resistivity, for $T > 182\text{K}$, based purely on a Debye temperature transition. On the other hand, a hysteresis between heating and cooling is often observed

below a first-order I-CDW to CDW transition. The absence of a thermal hysteresis, as in the case of $\text{Lu}_5\text{Ir}_4\text{Si}_{10}$, often leads to speculation that the transition either is of second order or has some “unconventional” origin.^{40,41} In our case, as shown in Fig 3b, the resistivity below 140K does not display a thermal hysteresis. This indicates that the 140K transition is likely a second-order CDW transition. According to this reasoning, the 200K transition is a first-order transition.

Note in Fig. 5 that the $1/T_1$ data for both orientations follow similar behavior as a function of temperature, except that the relaxation rates for $H \parallel c$ are about an order of magnitude faster compared to $H \perp c$. However, they approach almost the same value at room temperature. Above 200K, the temperature behavior differs: the $1/T_1$ value remains constant from room temperature to 200K for the parallel case while it precipitously drops for the perpendicular case. This would imply a constant relaxation mechanism that only exists in the parallel direction and is weakly dependent on temperature, while in the perpendicular direction, this mechanism monotonically diminishes until the temperature reaches 200K. The origin of this mechanism is not clear but it may be related to the topological nature of this family of systems which suppresses the relaxation channel when the field is applied parallel to the plane of the layers.^{54,55}

To analyze this further, let us suppose that the relaxation rates can be separated into electronic and phonon contributions:⁵³

$$1/T_1(k) = 1/T_1^{\text{el}}(k) + 1/T_1^{\text{ph}}(k)$$

where $k = \parallel, \perp$ are the magnetic field directions with respect to the crystal c-axis. The electronic contribution is magnetic in nature and is due to the spin scattering of the

conduction electrons. On the other hand, the phonon contribution is driven by changes in the lattice which works its way to the nuclear relaxation via quadrupolar effects. Due to the fact that the CDW energy gap we obtained below 140K is isotropic, it is reasonable to assume that the conduction band electronic contribution $1/T_1^{\text{el}}(k)$ is also isotropic, as well as the temperature dependence of $1/T_1^{\text{el}}(k)$ itself. We plot in the inset of Fig. 5 the differences in relaxation rates $\Delta 1/T_1 = 1/T_1(\parallel) - 1/T_1(\perp)$ between each field orientation. Here, we can clearly see that the anisotropy in relaxation is mainly due to phonon contribution along $H \parallel c$ direction, i.e., $\Delta 1/T_1 > 0$ at all temperatures. It starts small at room temperature, peaks at 200K and finally freezes as the sample is further cooled.

The positive value of $\Delta 1/T_1$ reveals that a stronger lattice vibration (phonons) is present in the $H \parallel c$ -axis measurements. This can be understood from the 2D layered structure of this material, where Bi-Bi bonds within the ab planes have stronger electron-phonon coupling effects than the ones along c-axis.⁵⁶ Our results are as expected, since the longitudinal relaxation $1/T_1(\parallel)$ is sensitive to fluctuations perpendicular to the direction of the magnetic field. Combining our high temperature observations from SAED and resistivity data, the $\Delta 1/T_1$ peak at 200K is likely a phonon mediated structural phase transition. At high temperatures, the temperature dependent behavior of $1/T_1$ is driven by its correlation with the lattice imperfections or the PLD. When the temperature reaches 200K, the lattice vibration becomes weak and a soft phonon is observed, resulting to a structural phase transition and a peak in relaxation. This is reminiscent of critical slowing down in spin systems where a peak in $1/T_1$ is observed when the system undergoes phase transition. From 200K to 140K, the electronic contribution becomes dominant and the phonon vibrations are further weakened. However, phonon vibrations are not entirely

absent and still contributes to the relaxation. In this range, some of the electronic charges are ordered with the underlying lattice and some are not, thus, there is a mixture of I-CDW and CDW phases. Since $1/T_1$ is an integration over the entire Fermi surface, it is possible that in this temperature range the Fermi surface only opened a small segment with mini CDW gaps. At 140K, a threshold is reached when the phonons are weak enough and the electronic charges becomes more commensurate with the underlying lattice. Consequently, the entire Fermi surface undergoes a gapped Peierls transition, thus completing the CDW (insulating) state.

The case for a Charge Density Wave in Bi₂Se₃

As discussed earlier, topological insulators such as Bi₂Se₃ and Bi₂Te₃ are expected to host density wave order due to their complex fermiology – in particular, strong Fermi surface nesting.^{21,22} Angle Resolved Photoemission Spectroscopy (ARPES) measurements show that Bi₂Se₃ has a hexagonally deformed Fermi surface. The two parallel segments in the hexagonal Fermi surface separated by $2k_F$ (where, k_F is the Fermi wavevector) can lead to strong nesting and density wave order. Given the topology of the surface states, the two parallel vectors \vec{k} and $-\vec{k}$ could also yield a Spin Density Wave (SDW). However, the Fermi surface is deformed only above 200meV, where bulk bands can become involved. Below 200meV, one finds a pure surface state with a circular constant energy contour.²¹ Thus, bulk states may contribute to Fermi surface deformation, leading to strong Fermi nesting. Shubnikov-de Haas measurements on Nb-Bi₂Se₃ have revealed evidence for a small extra Fermi pocket besides the main Fermi surface of Bi₂Se₃.³ Additionally, a first-

principles linear response calculation for Cu-Bi₂Se₃ has revealed a ‘prism-like’ fermi pocket at the Γ point, with opportunities for strong Fermi nesting.¹ Thus, theoretically speaking, the CDW transition reported here is not a surprising result.

When intercalated with Nb, Cu, or Sr, or when subjected to high pressure, Bi₂Se₃ becomes a superconductor with unconventional pairing.^{2,12-14} Strong electron correlations are often found in the vicinity of superconductivity^{17,18} although *sp* electrons in Bi₂Se₃ are weakly correlated. Xiangang and Sergey¹ suggest that unconventional superconductivity in intercalated layered systems such as Cu-Bi₂Se₃ might arise from an enhancement of electron-phonon coupling due to strong nesting at long wavelengths. At a certain wave vector q_0 , all pairing channels become degenerate and compete with each other. This singular electron phonon interaction with strong Fermi nesting at long wavelength can provide a large effective coupling constant favoring pseudo-triplet pairing of A_{2u} symmetry in intercalated Bi₂Se₃.¹ Thus, an interplay of strong spin-orbit coupling, unbroken time-reversal symmetry, and inversion symmetries with certain lattice distortions could lead to enhanced electron-phonon correlations and exotic superconducting states.

As described by Zhu et al⁵⁷, the origin of CDW is strongly related to dimensionality. They describe “Type-I” CDWs as quasi-1D systems with origins in traditional Peierls’ instability and Fermi Surface Nesting (FSN), with lattice distortion being a consequence of the electronic disturbance, as found in linear-chain compounds. Zhu et al assert that “Type-II” CDWs, in contrast, are driven by electron-phonon coupling (EPC) and not by FSN. In such cases, the electronic and lattice instabilities are intimately tied to each other with a phonon mode at q_{CDW} which goes to zero at the transition temperature T_{CDW} . This

second type does not require a metal-insulator transition associated with T_{CDW} . They further describe a “Type-III” case, where a charge modulation is found without the driving force of an FSN or EPC, and where the driving force is possibly electron correlations.

Most CDW occurs in quasi-1D or quasi-2D; our current understanding of CDW does not include all the complexities involved in the 3D case, where electron correlations are thought to play a primary role.⁵⁷ In this context, it is instructive to further discuss the possible effect of intercalation on k_F anisotropy between k_z versus k_x , k_y . Xiangang and Sergey¹ suggest that small changes in the position of Bi in the z-direction can modify the nesting vector $X(q) = \sum \delta(\varepsilon_k) \delta(\varepsilon_{k+q})$, where, ε_k and ε_{k+q} are the energy of states at/near the Fermi level. This nesting vector is largest for wavevector q along the Γ_z direction, when q is close to zero. This can lead to strong Fermi nesting, and strong electron-phonon coupling. Displacement along [001] at small qs (i.e., small momenta) breaks spatial inversion symmetry, lifts double degeneracy, and leads to a large electron-phonon coupling matrix element along this direction close to zone center. Further calculations by Xiangang and Sergey¹ and neutron scattering experiments by J. Wang, et al² show broad phonon linewidths for small qs , which could dominate electron-phonon coupling. Based on these arguments, we tentatively pose the possibility of the presence of a quasi-1D Peierls-type transition in the z-direction of Bi_2Se_3 .

Electron Diffraction

Room temperature selected area electron diffraction in Figures 1b, 2c, and 2d, taken along the [001] zone axis, displays the hexagonal symmetry that Bi_2Se_3 is known for.

This is indicated by labeled diffraction spots. Figures 1a, 2a, and 2b are bright field Transmission Electron Microscopy images showing the portions of the single crystal where the convergent electron beam was placed. Note the image in Fig. 2d, with the sample tilted slightly from zone axis. This clearly shows diffuse stripes between diffraction spots. As also discussed earlier, such diffuse scattering arises from incommensurate lattice distortion concomitant with an incommensurate charge density wave (I-CDW). We use this information, together with our observation of the opening up of a gap near 140K in bulk resistivity measurement and local microscopic measurement (NMR T_1), as evidence for a CDW transition at 140K.

Materials considerations

The somewhat elusive nature of superconductivity in single crystals of Cu-Bi₂Se₃, especially the variability of superconducting fraction and T_c to quenching temperature,^{25,26} is likely due to the high sensitivity of electron interactions to actual conditions of quenching and growth. The crystals discussed here were grown using a standard self-flux method, and a quenching temperature of 650C. The ideal topological insulator, Bi₂Se₃, has separate bulk and surface states. However, experimentally, intrinsic defects and disorder can be widely found in Bi₂Se₃ and intercalated/electron-doped Bi₂Se₃.^{9,39} Schneeloch et al²⁶ used different growth conditions to grow Cu doped Bi₂Se₃ superconductor and reported that high temperature quenching (above 560C) is essential for superconductivity, especially superconductivity with high diamagnetic shielding fraction. Other growth conditions either cause no SC or show weak diamagnetic shielding fraction. This is also our observation²⁵ in Cu-Bi₂Se₃. Schneeloch et al suggest that the quenching process either helps maintain a

primary intercalated phase or a secondary phase responsible for superconductivity. Huang et al show that high annealing temperature ($\sim 600^\circ\text{C}$) can cause intercalation of Bi_2 in Bi_2Se_3 .⁴⁴ Our results in this article indicate that high-temperature quenching (from above 650°C) leads to strong electron and lattice order, and to interesting electronic ground states such as a CDW or superconductivity.

X-ray diffraction (XRD) on powdered samples reveals that the a-axis value of our single crystal Bi_2Se_3 agrees with those of most other reports, but that the c-axis, at 28.66 \AA , is 0.02 \AA higher than the 28.64 \AA reported in most previous reports Bi_2Se_3 .^{30,58-59} Huang et al assert that a longer c-axis arises from unintentionally doped Bi-rich flux growth of Bi_2Se_3 where Bi forms a neutral metal Bi_2 layer intercalated into the van der Waals gap.³⁰ They also show that crystals with patches of intercalated Bi show high c-axis values of up to 28.65 \AA , close to the c-axis value of 28.66 \AA obtained from our Rietveld refinement. XRD results on our Bi_2Se_3 single crystals show no signs of the formation of metastable phases of staged $(\text{Bi}_2)_m(\text{Bi}_2\text{Se}_3)_n$. The solidification temperature of Bi_2Se_3 (705°C) is higher than the melting point of both pure Bi (271.4°C) and pure Se (220°C). Additionally, Se is a vapor above 685°C , which is below the solidification temperature of Bi_2Se_3 . Consequently, the stoichiometry of Bi_2Se_3 forming at the liquid-vapor interface can be highly dependent upon the vapor pressure of Se at 705°C . For high annealing temperature (around 600°C), partial decomposition might occur. Huang presumes that this is due to a large number of Se vacancies created in an evacuated environment, resulting in liquid Bi in the flux ending up in the van der Waals gaps rather than incorporating into a Bi-Se quintuple layer containing Se vacancies. Our crystals quenched at 650°C (above the high annealing temperature of 600°C that Huang claims results in Se

vacancies) could lead to Se vacancies and intercalated Bi. We surmise that, as there is not enough excess Bi to form the metastable phase of staged $(\text{Bi}_2)_m(\text{Bi}_2\text{Se}_3)_n$, excess Bismuth in our crystals forms randomly distributed Bi_2 inter-layers in the crystal. The resulting Bi-chains could help form a quasi-1D Peierls-type transition or a quasi-2D type CDW.^{30, 57,}
⁶⁰In summary, specific growth conditions can drive the observation of a CDW or superconductivity in Bi_2Se_3 . Further work is needed in this direction.

In addition to the discussion of Fig 7, comparison of our temperature dependent resistivity data and Knight shift of central transition with Young's sample #2 and sample #3 further supports that crystal growth conditions have important impact on the electronic behavior of samples. All the three samples (ours, Young's #2, and #3) were grown under different conditions. Young's ARPES results show that the Fermi level of their sample #2 lies within the bottom of the conduction band and that of sample #3 lies in the surface state, far below the conduction band. Since both our resistivity data and Knight shift values are in between Young's two samples (but closer to #2), it is likely that the Fermi level of our sample sits close to but lower than the Fermi level of their sample #2.

To conclude, we have presented evidence for the first direct experimental observation of charge density wave (CDW) order in Bi_2Se_3 . Diffuse streaks in SAED measurements indicate the presence of an incommensurate periodic lattice distortion at room temperature, reminiscent of an incommensurate charge density wave (I-CDW). A metal to insulator transition at 140K in resistivity measurements indicates the opening of a CDW-like energy gap. NMR spin-lattice relaxation rate $1/T_1$ measurements further confirm the presence of the 140K transition with an energy gap of about 8meV. Using

this, together with thermal hysteresis studies of resistivity, we conclude that Bi_2Se_3 displays an unconventional second-order quasi-1D CDW transition temperature at 140K. $1/T_1$ also reveals another transition near 200K, which shows an anisotropy in comparison of $H\parallel c$ to $H\perp c$ measurements. The differences in relaxation rates $\Delta 1/T_1$ from $H\parallel c$ to $H\perp c$ further signify this transition and indicate that there is a stronger lattice vibration (phonons) present in the $H\parallel c$ -axis measurements. Combining our high temperature observations from SAED and resistivity data, the transition at 200K is likely a phonon mediated structural phase transition. Furthermore, we also discuss how growth methods could promote the formation of a CDW. We suggest that strongly correlated ground states are present in Bi_2Se_3 crystals grown with a high annealing and quenching temperature. In this scenario, the higher temperature growth conditions result in self-intercalation of Bi/Se into Bi_2Se_3 , leading to a Periodic Lattice Distortion and producing, in turn, a Charge Density Wave transition. Thus, further studies are required in order to elucidate the dependence of electronic correlations on growth conditions, and to the occurrence of interesting ground states such as CDW and superconductivity.

Methods

Single crystals of Bi_2Se_3 were prepared by melting high purity (99.999%) powders of Bi and Se. Stoichiometric mixtures of 2.5 g were sealed into high-quality quartz tubes in vacuum after being weighed and sealed in an inert glove box, taking extreme care to never expose to air. The mixtures sealed in quartz tubes were heated up to 850 C and held for 20 hours. They were then cooled to 650 C at 0.1 C/min, followed

by quenching into ice water from high temperature. This yielded large, shiny single crystals which were easily cleaved along the ab plane.

Powder X-ray diffraction data were collected from pieces of single crystals powdered inside an inert glove box. Rietveld refinement was performed using GSAS (General Structure Analysis System) and the EXPGUI interface. Selected Area Electron Diffraction (SAED) was performed at room temperature with a Hitachi H-9000NAR high resolution transmission electron microscope (HRTEM) operated at 300 kV. Four-probe resistivity measurements were performed with varying temperature and magnetic field using a Quantum Design Physical Property Measurement System (PPMS).

Pulsed ^{209}Bi NMR (Nuclear Magnetic Resonance) measurements were performed on a Bi_2Se_3 single crystal of crystal size $\sim 0.94 \times 0.58 \times 0.41$ cm placed inside a home-built probe in an 11-Tesla Helium cryostat. The single crystal of Bi_2Se_3 was studied with magnetic field oriented in two directions, $H \perp c$ and $H \parallel c$. Spin-echo signals for ^{209}Bi NMR spectra were processed using the summed Fourier transform method, with field swept from 9.7T to 10.5T. Spin Lattice relaxation time T_1 measurements in both $H \parallel C$ and $H \perp C$ directions were performed at stabilized temperature points varying between 1.6K and 300K. We employed a train of RF pulses on the central transition to saturate the magnetization followed by variable delays and integrate the spin-echoes to map the magnetization recovery.

The magnetization recovery $M(t)$ is fitted with a stretched single exponential, appropriate for the initial condition where the quadrupolar satellites are completely saturated⁶¹:

$$M(t) = M_{\infty} \left[1 - e^{-(t/T_1)^{\beta}} \right]$$

where the parameter β allows for a distribution of T_1 .

Magnetization recovery $M(t)$ can either be fitted by a master equation or a stretched exponential equation.^{61,62} Stretched exponential fitting is used when there is a continuous distribution of relaxation rates. In our measurement set-up, we used a pulse train to saturate all the NMR lines. Although the signal does not saturate completely, we find that a stretched single exponential fits our data better than using the master equation.

Author Contributions

YL and CP grew samples and YL performed all measurements. Electron diffraction was performed by YL and MAS, led by MAS. YL and SR performed NMR measurements under the direction of AR; CP and AD assisted YL in analysis. YL wrote the first draft of the manuscript under the direction of PG, with assistance from AR, CP and AD and reviewed by AR. PG provided supervision of the overall project.

Acknowledgements

We gratefully acknowledge support from Steve Hardcastle of the Advanced Analysis Facility, and Prof. M. Gajdarziska Josifovska for the use of the Hitachi H-9000NAR high resolution transmission electron microscope in the HRTEM facility. We acknowledge an earlier AFOSR MURI grant to PG. A portion of this work was performed at the National High Magnetic Field Laboratory, which is supported by the National Science Foundation Cooperative Agreement No. DMR-1644779 and the state of Florida.

Competing interests

The authors declare no competing interests.

REFERENCES

- [1] Wan, X. & Savrasov, S. Turning a band insulator into an exotic superconductor. *Nat Commun* **5**, 4144 (2014).
- [2] Wang, J. *et al.* Evidence for singular-phonon-induced nematic superconductivity in a topological superconductor candidate $\text{Sr}_{0.1}\text{Bi}_2\text{Se}_3$. *Nat Commun* **10**, 2802 (2019).

- [3] Lawson, B. J. *et al.* Multiple Fermi surfaces in superconducting Nb-doped Bi₂Se₃ *Phys. Rev. B* **94**, 041114(R) (2016).
- [4] Hecker, M. & Schmalian, J. Vestigial nematic order and superconductivity in the doped topological insulator Cu_xBi₂Se₃. *npj Quant Mater* **3**, 26 (2018).
- [5] Matano, K. *et al.* Spin-rotation symmetry breaking in the superconducting state of Cu_xBi₂Se₃. *Nature Phys* **12**, 852–854 (2016).
- [6] Shen, J. *et al.* Nematic topological superconducting phase in Nb-doped Bi₂Se₃. *npj Quant Mater* **2**, 59 (2017).
- [7] Xia, Y. *et al.* Observation of a large-gap topological-insulator class with a single Dirac cone on the surface. *Nature Phys* **5**, 398–402 (2009).
- [8] Hsieh, D. *et al.* A tunable topological insulator in the spin helical Dirac transport regime. *Nature* **460**, 1101–1105 (2009).
- [9] Hor, Y. S. *et al.* p-type Bi₂Se₃ for topological insulator and low-temperature thermoelectric applications. *Phys. Rev. B* **79**, 195208 (2009)
- [10] Tumelero M. A., Faccio R. & Pasa A. A. The role of interstitial native defects in the topological insulator Bi₂Se₃. *J. Condens. Matter Phys.* **28**, 425801 (2016).
- [11] Lahoud, E. *et al.* Evolution of the Fermi surface of a doped topological insulator with carrier concentration. *Phys. Rev. B* **88**, 195107 (2013)
- [12] Kirshenbaum, K. *et al.* Pressure-Induced Unconventional Superconducting Phase in the Topological Insulator Bi₂Se₃. *Phys. Rev. Lett.* **111**, 087001 (2013).
- [13] Sasaki, S. *et al.* Topological Superconductivity in Cu_xBi₂Se₃. *Phys. Rev. Lett.* **107**, 217001 (2011)
- [14] Asaba, T. *et al.* Rotational Symmetry Breaking in a Trigonal Superconductor Nb-doped Bi₂Se₃. *Phys. Rev. X* **7**, 011009 (2017)
- [15] Kohama, Y. *et al.* Possible Unconventional Superconductivity in Iron-Based Layered Compound LaFePO: Study of Heat Capacity. *J. Phys. Soc. Jpn.* **77**, 094715 (2008)
- [16] Kiss, T. *et al.* Photoemission Spectroscopic Evidence of Gap Anisotropy in an f-Electron Superconductor. *Phys. Rev. Lett.* **94**, 057001
- [17] Stewart, G. R. Unconventional superconductivity. *Adv. Phys.* **66**, 75-196 (2017)

- [18] Davis, J. C. S. & Lee, D.-H. Concepts relating magnetic interactions, intertwined electronic orders, and strongly correlated superconductivity. *Proc. Natl Acad. Sci. USA* **110**, 17623–17630 (2013)
- [19] Biswas, D., Thakur, S., Balakrishnan, G. & Maiti, K. Exceptional surface and bulk electronic structures in a topological insulator, Bi_2Se_3 . *Sci Rep* **5**, 17351 (2015).
- [20] Hor, Y. S. *et al.* Superconductivity in $\text{Cu}_x\text{Bi}_2\text{Se}_3$ and its implications for pairing in the undoped topological insulator. *Phys. Rev. Lett.* **104**, 057001 (2010).
- [21] Kuroda, K. *et al.* Hexagonally Deformed Fermi Surface of the 3D Topological Insulator Bi_2Se_3 . *Phys. Rev. Lett.* **105**, 076802 (2010).
- [22] Fu, L. Hexagonal Warping Effects in the Surface States of the Topological Insulator Bi_2Te_3 . *Phys. Rev. Lett.* **103**, 266801 (2009).
- [23] Zhang, H., Liu, C.-X., & Zhang, S.-C. Spin-Orbital Texture in Topological Insulators. *Phys. Rev. Lett.* **113**, 066801 (2013).
- [24] Koski, K. J. *et al.* Chemical intercalation of zerovalent metals into 2D layered Bi_2Se_3 nanoribbons. *JACS* **134**, 13773–13779 (2012).
- [25] Smith, Nathaniel P., "Crystal Growth and Manipulation of Intercalated Chalcogenides as Superconductors and Topological Insulators" PhD Thesis, University of Wisconsin Milwaukee (2018).
- [26] Schneeloch, J. A., Zhong, R. D., Xu, Z. J., Gu, G. D., and Tranquada, J. M., Dependence of superconductivity in $\text{Cu}_x\text{Bi}_2\text{Se}_3$ on quenching conditions. *Phys. Rev. B* **91**, 144506 (2015)
- [27] Wilson, J. A., Di Salvo, F. J. & Mahajan, S. Charge-density waves and superlattices in metallic layered transition-metal dichalcogenides. *Adv. Phys.* **24** 117–201(1975)
- [28] Wilson, J. A., Di Salvo, F. J. & Mahajan, S. Charge-density waves in metallic, layered, transition-metal dichalcogenides. *Phys. Revs. Lett.* **32** 882 (1974)
- [29] Wang, M. & Koski, K. J. Polytypic phase transitions in metal intercalated Bi_2Se_3 . *J. Phys. Condens. Matter* **28**, 494002 (2016).
- [30] Huang, F.-T. *et al.* Nonstoichiometric doping and Bi antisite defect in single crystal Bi_2Se_3 . *Phys. Rev. B* **86**, 081104(R) (2012).
- [31] Dai, J. *et al.* Toward the Intrinsic Limit of the Topological Insulator Bi_2Se_3 . *Phys. Rev. Lett.* **117**, 106401(2016)

- [32] Nath, D., Singh, F., Das, R. X-ray diffraction analysis by Williamson-Hall, Halder-Wagner and size-strain plot methods of CdSe nanoparticles- a comparative study. *Mater. Chem. Phys.* **239**, 122021 (2020)
- [33] Shafi, P. M., Bose, A. C. Impact of crystalline defects and size on X-ray line broadening: A phenomenological approach for tetragonal SnO₂ nanocrystals. *AIP Advances* **5**, 057137 (2015)
- [34] Williams, P. M., Scruby, C., Clark, W. & Parry, G. Charge density waves in the layered transition metal dichalcogenides. *J. Phys. Colloques.* **37** C4-139–150(1976)
- [35] McMillan, W. L. Landau theory of charge-density waves in transition-metal dichalcogenides. *Phys. Rev. B* **12** 1187 (1975)
- [36] Di Salvo, F. J. & Maurice Rice, T. Charge-density waves in transition-metal compounds. *Phys. Today* **32** 32 (1979)
- [37] Li, Y., Smith, N. P., Rexhausen, W., Schofield, M. A. & Guptasarma, P. Possible lattice and charge order in Cu_xBi₂Te₂Se. *J. Phys. Mater.* **3** 015008 (2020)
- [38] Duvjir, G. *et al.* Emergence of a Metal–Insulator Transition and High-Temperature Charge-Density Waves in VSe₂ at the Monolayer Limit. *Nano Letters* **18** (9), 5432-5438 (2018)
- [39] Craven, R. A. & Meyer, S. F., Specific heat and resistivity near the charge-density-wave phase transitions in 2H–TaSe₂ and 2H–TaS₂. *Phys. Rev. B* **16**, 4583 (1977)
- [40] Welsch, J. *et al.* Second-order charge-density-wave transition in single crystals of La₃Co₄Sn₁₃. *Phys. Rev. Materials* **3**, 125003 (2019)
- [41] Kuo, Y.-K., Lue, C. S., Hsu, F. H., Li, H. H. & Yang, H. D. Thermal properties of Lu₅Ir₄Si₁₀ near the charge-density-wave transition. *Phys. Rev. B* **64**, 125124 (2001)
- [42] Zong, A. *et al.* Ultrafast manipulation of mirror domain walls in a charge density wave. *Sci. Adv.* **4**, 5501 (2018).
- [43] Wezel, J. V., Nahai-Williamson, P., and Saxena S.S. Exciton-phonon-driven charge density wave in TiSe₂. *Phys. Rev. B* **81**, 165109 (2010).
- [44] Sugawara, K. *et al.* Unconventional charge-density-wave transition in monolayer 1T-TiSe₂. *ACS Nano* **10**, 1341 (2015).
- [45] Séamus Davis, J. C. & Lee, D.-H. Concepts relating magnetic interactions, intertwined electronic orders, and strongly correlated superconductivity. *PNAS.* **110**, 17623-17630 (2013)

- [46] Berthier, C., Jérôme, D., Molinié, P. *J. Phys. C: Solid State Physics*, **11**, 797 (1978)
- [47] Ohno, T., Kishimoto, Y., Miyatani, K. *Physica B (Amsterdam)* **230**, 988 (1997)
- [48] Tsuda, T., Kitaoka, Y., Yasuoka, H. *Physica B+C (Amsterdam)* **105**, 414 (1981)
- [49] Wada, S., Alloul, H., Molinié, P. Proton spin-lattice relaxation time in the superconducting intercalation complex $\text{Tas}_2(\text{pyridine})^{1/2}$. *J. Physique Lett.* **39**, 243-247 (1978)
- [50] Yogi, M., Higa, N., Niki, H., Kawata, T., Sekine, C. ^{75}As -NQR study of the hybridization gap semiconductor $\text{CeOs}_4\text{As}_{12}$. *J. Phys.: Conf. Ser.* **683** 012030 (2016)
- [51] Gruner, G. The dynamics of charge-density waves. *Rev. Mod. Phys.* **60**, 1129-undefined (1988).
- [52] Nisson, D. M. *et al.* Nuclear magnetic resonance as a probe of electronic states of Bi_2Se_3 . *Phys. Rev. B* **87**, 195202 (2013)
- [53] Young, B.-L. *et al.* Probing The Bulk Electronic States of Bi_2Se_3 Using Nuclear Magnetic Resonance. *Phys. Rev. B* **86**, 075137 (2012)
- [54] Fal'ko, V. & Jungwirth T. Orbital effect of an in-plane magnetic field on quantum transport in chaotic lateral dots. *Phys. Rev. B* **65**, 081306 (2002)
- [55] Taskin, A.A., Legg, H.F., Yang, F. *et al.* Planar Hall effect from the surface of topological insulators. *Nat Commun* **8**, 1340 (2017).
- [56] Zhu, X., *et al.* Electron-Phonon Coupling on the Surface of the Topological Insulator Bi_2Se_3 Determined from Surface-Phonon Dispersion Measurements. *Phys. Rev. Lett.* **108**, 185501 (2012)
- [57] Zhu, X., Cao, Y., Zhang, J., Plummer, E. W. & Guo, J. Classification of charge density waves based on their nature. *Proc. Natl Acad. Sci. USA* **112**, 2367–2371 (2015).
- [58] Chiatti, O. *et al.* 2D layered transport properties from topological insulator Bi_2Se_3 single crystals and micro flakes. *Sci Rep* **6**, 27483 (2016).
- [59] Martinez, G. *et al.* Determination of the energy band gap of Bi_2Se_3 . *Sci Rep* **7**, 6891 (2017).
- [60] Zhu, X., Guo, J., Zhang, J., Plummer, E.W. Misconceptions associated with the origin of charge density waves. *Adv. Phys.: X*, **2**, 622-640 (2017)
- [61] Narath, A., Nuclear Spin-Lattice Relaxation in Hexagonal Transition Metals: Titanium. *Phys. Rev.* **162**, 320 (1967)

[62] Suter, A., Mali, M., Roos, J., Brinkmann, D. Mixed magnetic and quadrupolar relaxation in the presence of a dominant static Zeeman Hamiltonian. *J. Phys: Condens. Matter*, **10**, 5977-5994 (1998)